HHS Public Access

Author manuscript

Bioconjug Chem. Author manuscript; available in PMC 2020 January 02.

Published in final edited form as:

Bioconjug Chem. 2019 June 19; 30(6): 1724–1733. doi:10.1021/acs.bioconjchem.9b00262.

Gold Nanoparticles Disrupt Tumor Microenvironment - Endothelial Cell Crosstalk to Inhibit Angiogenic Phenotypes *in vitro*

Yushan Zhang[†], **Xunhao Xiong**[†], **Yanyan Huai**[†], **Anindya Dey**[‡], **Nazir Md Hossen**[†], **Ram Vinod Roy**[†], **Chandra Kumar Elechalawar**[†], **Geeta Rao**[†], **Resham Bhattacharya**[‡,§], **Priyabrata Mukherjee**[*,†,§]

[†]Department of Pathology, The University of Oklahoma Health Sciences Center, Oklahoma City, Oklahoma 73104, USA

[‡]Department of Obstetrics and Gynecology, The University of Oklahoma Health Sciences Center, Oklahoma City, Oklahoma 73104, USA

[§]Peggy and Charles Stephenson Cancer Center, The University of Oklahoma Health Sciences Center, Oklahoma City, Oklahoma 73104, USA

Abstract

It is currently recognized that perpetual crosstalk among key players in tumor microenvironment such as cancer associated fibroblasts (CAFs), cancer cells (CCs) and endothelial cells (ECs) play a critical role in tumor progression, metastasis and therapy resistance. Disruption of the crosstalk may be useful to improve the outcome of therapeutics for which limited options are available. In the current study we investigate a use of gold nanoparticles (AuNPs) as a therapeutic tool to disrupt the multicellular crosstalk within the TME cells with an emphasis on inhibiting angiogenesis. We demonstrate here that AuNPs disrupt signal transduction from TME cells (CAFs, CCs and ECs) to ECs and inhibit angiogenic phenotypes *in vitro*. We demonstrate that conditioned media (CM) from ovarian CCs, CAFs or ECs themselves induce tube formation and migration of ECs *in vitro*. Migration of ECs is also induced when ECs are co-cultured with CCs, CAFs or ECs. In contrast, CM from the cells treated with AuNPs, or co-cultured cells pre-treated with AuNPs demonstrate diminished effects on ECs tube formation and migration. Mechanistically, AuNPs deplete ~95% VEGF165 from VEGF single-protein solution, and remove up to ~45% of VEGF165 from CM, which is reflected on reduced activation of VEGF-Receptor 2 (VEGFR2) as compared to control CM. These results demonstrate that AuNPs inhibit angiogenesis via blockade of VEGF-VEGFR2 signaling from TME cells to endothelial cells.

[*]Corresponding Author: Priyabrata Mukherjee PhD., Professor, Department of Pathology, Experimental Pathology, Peggy and Charles Stephenson Endowed Chair in Cancer Laboratory Research, College of Medicine and Stephenson Cancer Center, 975 NE 10th Street, BRC-1409B, Oklahoma City, OK 73104. Priyabrata-Mukherjee@ouhsc.edu, Phone: 405-271-1133. Fax: 405-271-2472.

Supporting Information

Physicochemical characterizations of AuNPs; Tube formation of HMEC treated with CM from CC, CAF or EC cells; Migration of HUVEC treated with cell CM, or co-cultured with cells treated with AuNP; and Typical standard curve for VEGF165 ELISA quantification and the calculation of sample VEGF165.

The authors declare no conflicts of interest.

Graphical Abstract

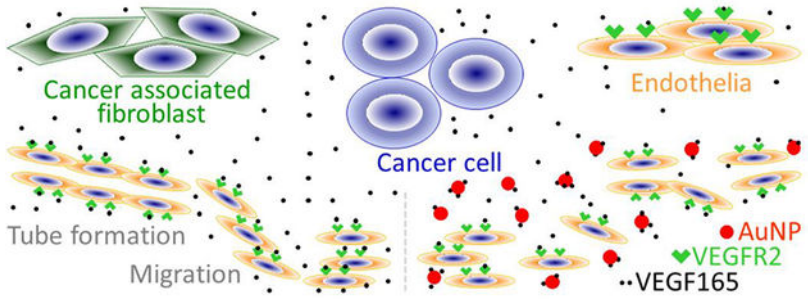

Keywords

Angiogenesis; Conditioned media; Epithelial ovarian cancer; Gold nanoparticle; Tumor microenvironment; VEGF

INTRODUCTION

Epithelial ovarian cancer (EOC) is one of the leading causes of cancer-related death in women.[1,2] Tumor stroma, consisting of cancer associated fibroblasts (CAFs), endothelial cells (ECs), extracellular matrix, among other components, has been realized as a major contributor to EOC progression and therapy resistance.[3] Tumor stroma not only provides cancer cells (CCs) with physical shelter and barrier, but also stimulates cancer cells proliferation, migration and invasion via cell-cell communication. Likewise, the crosstalk between cancer cells and stromal cells, and that among stromal cells in the tumor microenvironment (TME) maintains stromal cells in an activated state, thus fostering tumor aggressiveness.[4,5] By limiting drug access, secreting growth factors, cytokines, chemokines or new ligands that promote cancer cell survival, growth or metastasis, or reducing drug receptors in cancer cells, stromal cells can mediate the resistance to anticancer therapies and disease recurrence.[6] Therefore, disrupting the interactions among TME cells, i.e., cancer cells and stromal cells,[7] may serve as an alternative strategy to treat EOC.

Unmodified gold nanoparticles (AuNPs) have been demonstrated to possess intrinsic inhibitory property to a variety of cancer cells and stromal cells, as well as the interaction between different cell types in TME. Gold nanoparticles up-regulated p21 and p27 in multiple myeloma cell lines and caused cell cycle arrest and inhibition of proliferation.[8] AuNPs reduced the viability and migration of cervix adenocarcinoma cells,[9] reversed epithelial mesenchymal transition (EMT) in melanoma cells and prevented melanoma metastasis to lungs.[10] In line with these, the particles disrupted MAPK signaling, reversed EMT and blocked tumor growth and metastasis in EOC models.[11] For vascular smooth muscle cells, the nanoparticles reduced their migration, adhesion and proliferation by restraining FAK phosphorylation.[12] It was shown that AuNPs not only induced autophagy in endothelial cells and impeded *in vitro* tube formation,[13] but also obstructed retinal[13,14] and choroidal[15] neovascularization in mice. By binding proangiogenic heparin-binding growth factors (HB-GFs), such as vascular endothelial growth factor-165 (VEGF165) and basic fibroblast growth factor (bFGF), gold nanoparticles retarded endothelia or fibroblasts

proliferation *in vitro* and angiogenesis *in vivo*.[16–18] Noticeably, AuNPs disrupted the crosstalk between pancreatic cancer cells and pancreatic stellate cells (the pancreatic cancer associated fibroblasts) via alteration of the cell secretomes, inhibited proliferation and migration of both cell types, and impeded tumor growth in animals.[19] Mechanically, AuNPs have strong affinity to -SH- and -NH2-containing molecules and allow preferentially binding of cysteine/lysine-rich proteins to them.[20] Such binding then altered the structures and functions of the proteins, as in the case of HB-GFs. The inhibitory effect of AuNPs was partly due to the change in HB-GFs conformation/configuration by the nanoparticles, whereas the conformations of non-HB-GFs remained unaffected.[17,18] The observations above strongly suggested that AuNPs could serve as a promising tool to disrupt the crosstalk among cancer cells, endothelial cells, and fibroblasts in TME.

ECs are a major cell type in the TME. Their interactions with CCs, CAFs and other TME constituents are key initiators or/and regulators for tumor angiogenesis, invasion and metastasis.[21–23] We observed that AuNPs inhibited angiogenesis in EOC mouse xenografts,[11,24] but the mechanisms underlying have not been elucidated. We postulated that interrupting the interactions between endothelial cells and other cells in ovarian TME by AuNPs is one of the mechanisms. In this study, we investigated the effects of ovarian TME cells on ECs angiogenic phenotypes *in vitro*, and whether and how AuNPs perturb the processes.

RESULTS

Synthesization and Characterization of 20 nm AuNPs.

Our previous work showed that AuNPs of 20 nm in diameter exhibited the highest efficacy in inhibiting VEGF165 induced proliferation of HUVECs.[18] So we synthesized 20 nm AuNPs and characterized their physicochemical properties. The AuNPs showed the typical size of around 20 nm in diameter (Figure S1A and S1D), zeta potential as about 45 mV (Figure S1B), and a surface-plasmon resonance band centered at 522 nm (Figure S1C). We used these AuNPs in this study and used them within 2 weeks after preparation.

Isolation and Characterization of Primary Ovarian CAFs.

To investigate the interaction between CAFs and ECs, we isolated primary ovarian CAFs using 26 freshly resected ovarian cancer tissues. 2–3 days after the placing of tissue blocks to culture plates, some large, flat, and spindle-shaped cells appeared (passage 1, Figure 1A) surrounding the tissue blocks from 15 patients. The cells from 12 patients grew to 90%–100% confluent within 3 weeks and were passaged 3 times to larger culture dishes. The cells (passage 4), named TAF1–26, were then subjected to verification by western blotting and immunofluorescence staining for expression of α-SMA (CAF specific marker),[25] fibronectin (highly expressed in CAF)[25] and E-cadherin (epithelium marker, Figure 1B and 1C).[26] α-SMA is widely considered as the most reliable CAF specific marker and has been routinely used to identify CAFs.[27,28] Fibronectin is produced by a variety of cell types, including fibroblasts and epithelial cells, but highly expressed in CAFs.[29] E-cadherin is expressed in normal epithelial cells and well-differentiated cancer cells, but is lost in invasive tumor.[30] This panel of cell markers enables us to obtain ovarian CAFs, but not epithelial cells and

other cell types. 9 TAFs expressed both α-SMA and fibronectin, but not E-cadherin, demonstrating their CAF properties. These cells provided a suitable model for assessing the crosstalk between ovarian CAFs and ECs. We used TAF18 and TAF19 in this study based on their significant expressions of α-SMA and fibronectin, and no expression of E-cadherin (Figure 1).

Conditioned Medium (CM) of AuNPs Treated CCs, CAFs or ECs Inhibit Tube Formation of ECs.

To simulate ovarian TME cells effect on ECs behaviors, we investigated the effects of ovarian CC, ovarian CAF or EC cells on ECs *in vitro* tube formation, and whether AuNPs can interrupt the process. We firstly prepared CM from CP20, OV90, OVCAR4, TAF18, TAF19, HMEC and HUVEC cells treated with or without 40μg/ml AuNPs as described in Experimental Procedures and illustrated in Figure 2A, and used them for the following assays.

Incubation of HUVEC with the CM from non-treated cells (CM Con) resulted in 1.7 (TAF19 CM Con) to 3.4 (OV90 CM Con) fold increases in tube formation compared to PBS (Figure 3). However, HUVEC tube formation was significantly decreased when treated with CM from AuNPs-treated cells (CM NP), compared to CM from non-treated cells. The decreases were from 33.5% (CM from HMEC, NP vs Con) to 47.9% (CM from TAF18, NP vs Con) (Figure 3D–3F). Similar effects were also observed in HMEC, where a 2.6 (CP20 CM Con) to 4.1 (OV90 CM Con) fold increases of tube formation were resulted due to treatment by CM from non-treated cells compared to PBS. HMEC tube formation was reduced by 33.5% using HMEC CM NP and 48.3% using OVCAR4 CM NP when compared with respective control CMs (Figure 3G–3I, S2). These results demonstrated that ovarian TME cells induced ECs tube formation and treatement with AuNPs impaired that ability.

CM of CCs, CAFs or ECs Treated with AuNPs, or AuNPs in Co-culture System, Inhibit ECs Migration.

We then investigated the effect of ovarian CC, ovarian CAF or EC cells on another angiogenic cascade phenotype, migration, and its perturbation by AuNPs using both CM (Figure 2A) and co-culture system (Figure 2B). The CM from CP20, OV90, OVCAR4, TAF18, TAF19, HMEC and HUVEC cells treated with or without 40μg/ml AuNPs were prepared as described in Experimental Procedures and illustrated in Figure 2A, diluted 1:1 with PBS, and added 700μl to the outwell to induce the migration of ECs seeded to the inserts. In co-culture system, the migration-inducing cells (CC, CAF or EC) were seeded to the outwells, treated with or without 40 μg/ml AuNPs in SFM for 36h, and then co-cultured with EC seeded onto the inserts. Both CM and co-cultured cells stimulated ECs migration compared to PBS, whereas AuNPs exhibited an inhibitory effect (Figure 4 and S3). Control CM (no nanoparticle treatment) treatment caused 3.7 (HUVEC migration by HMEC CM Con) to 8.9 (HUVEC migration by OV90 CM Con) fold increase in migration compared to PBS. Importantly, CM collected from AuNPs-treated cells decreased migration of HUVECs by 21.9% using OVCAR4 CM NP and 53.9% using OV90 CM NP (Figure 4B and 4C). Similarly, in co-culture system, CC, CAF or EC cells promoted ECs migration, while AuNPs inhibited the ability of TME cells to induced EC migration (Figure 4E and 4F). Non-

treated co-cultured cells increase the migration of ECs by 2.6 (HMEC migration by co-cultured CP20) to 15.9 (HUVEC migration by co-cultured HMEC) folds, whereas AuNP-treated co-cultured cells inhibit the migration by 22.9% (HMEC migration by co-cultured OV90 treated with AuNPs) to 48.6% (HUVEC migration by co-cultured OVCAR4 treated with AuNPs) compared with corresponding Controls. Collectively, these results showed that ovarian TME cells promote ECs migration, whereas AuNPs disrupt such effects.

CCs, CAFs or ECs Secrete VEGF That Can Be Removed by AuNPs.

VEGF is a major regulator for endothelial cell function and angiogenesis.[31,32] Our previous work showed that extrogenous recombinant VEGF165 can bind to AuNPs and such binding decreases its stimulatory effect.[16–18] We thus asked whether VEGF165 may be involved in the signaling from ovarian CCs, ovarian CAFs or ECs to ECs in our expeimental setting, and whether AuNPs may remove the VEGF165 from action. We used a PeproTech ELISA kit that can detect natural and/or recombinant VEGF165 within the range of 16–1000pg/ml to quantify VEGF165 in cell CM or VEGF single-protein solutions. Results showed that all the cells secrete VEGF165 at different levels, with the ranking OVCAR4 (565.8 pg/ml) > CP20 (467.2) > OV90 (159.0)> TAF18 (120.2) ≈ TAF19 (127.2) > HMEC (97.0) ≈ HUVEC (92.4) (Figure 5B: 0 μg/ml AuNPs, Figure S4). AuNPs drastically cleared exogenous recombinant VEGF165 from the single-protein solutions if incubated together overnight (Figure 5A): 20 μg/ml AuNPs depleted 92.8% VEGF165, whereas 40 μg/ml AuNPs remove 95.2% VEGF165. When AuNPs of these concentrations were incubated with cells in culture for 48 h, VEGF165 levels in cell CM were also dropped dose-dependently (Figure 5B: 20, 40 μg/ml AuNP), even though the efficacy of the clearance was lower than that for VEGF165 single-protein solutions, which is not unexpected due to the competition from other cellular proteins: 20 μg/ml AuNPs removed 3.8% (OVCAR4) to 26.9% (TAF19) VEGF165 from the CM, whereas 40 μg/ml AuNPs remove 12.3% (OVCAR4) to 45.6% (HMEC) VEGF165. These results showed that ovarian TME cells secreted VEGF165, and AuNPs depleted the endogenous VEGF165 from cell CM at least by directly binding.

CM of CCs, CAFs or ECs Treated with AuNPs Inhibit VEGFR2 Activation.

To further demonstrate that blocking of VEGF signaling is one of the mechanisms by which AuNPs interrupted the effects of ovarian CCs, ovarian CAFs or ECs on ECs, we checked the activation of VEGFR2, a major receptor for VEGF,[31,32] by cell CM. Treatment of starved HUVECs or HMECs with the cell CM phosphorylated VEGFR2 (Figure 5C), but the CM from cells pretreated with AuNPs demonstrated a less extent of activation of VEGFR2. Taken together, our results showed that ovarian TME cells stimulated EC *in vitro* angiogenic phenotypes such as endothelial tube formation and migration, whereas AuNPs inhibited those effects by inhibition of VEGF signaling from the TME cells to EC cells (Figure 5D).

DISCUSSION

In order to gain insight on how multicellular crosstalk in the tumor microenvironment promotes cancer progression and metastasis, in the current study we focused on a role of multicellular crosstalk in stimulating angiogenic phenotypes and its perturbation by gold nanoparticles. We demonstrated that the conditioned media of non-treated cancer cells,

cancer associated fibroblasts, or endothelial cells promoted *in vitro* tube formation and migration of endothelial cells, but the conditioned media collected from AuNP-treated cells showed diminished effects. VEGF165 levels in the CM from AuNP-treated cells were lower than those in the CM from non-treated cells. Consequently, activation of endothelial cell VEGFR2 was inhibited by CM from AuNP-treated cells when compared with non-treated cells. These results suggested that AuNPs inhibited *in vitro* angiogenic phenotypes via blockade of VEGF-VEGFR2 signal transduction from TME cells to endothelial cells (Figure 5D) and partially explained our previous observations that AuNPs inhibited *in vivo* angiogenesis of EOC mouse xenografts.[11,24]

VEGF-VEGFR2 is a key signaling pathway in physiological and pathological angiogenesis.[31–33] VEGF is secreted by many cell types in TME, including cancer cells, CAFs and immune cells.[25,34] It was also reported to be expressed by *in vitro* cultured endothelial cells,[35,36] even though undetectable *in vivo*.[37] Phosphorylation of VEGFR2 by VEGF activates PLCγ-ERK1/2 pathway, PI3K-AKT pathway, SRC pathway, p38 MAPK pathway and STAT proteins, regulating endothelial cell survival, morphology, migration, proliferation, junctions, and vascular development, permeability, barrier function, and vasomotion.[32] Our results suggest that AuNPs interupted the canonical VEGF-dependent VEGFR2 signalling as both VEGF165 level and VEGFR2 phosphorylation were downregulated by AuNPs. However, possibilities that AuNPs might interupt the non-canonical non-VEGF-dependent activation of VEGFR2 by factors such as gremlins, galectins, lactate, low-density lipoproteins, high-density lipoproteins or even mechanical forces,[32,38] could not be ruled out. Using antibody arrays, we previously detected the changes of expression of a number of angiogenesis related proteins in the CM of ovarian cancer cells, pancreatic cancer cells, and pancreatic stellate cells treated with AuNPs. Among the most significantly changed proteins are AREG, bFGF, CCL2, CD26, ColXVIII, EG-VEGF, endostatin, HGF, IL8, MMP8, MMP9, PlGF, Serpin E1, TGFβ1, THBS1,TSG14 and uPA.[11,19] These may help to explain why the tube formation and migration of HUVECs and HMECs (Figure 3 and 4) are not so corresponding to VEGF levels in the CM (Figure 5).

VEGF165 binds to AuNPs with its heparin-binding domain.[17] In single-protein solution, the efficiency of VEGF165 clearance by AuNPs reaches 95%,[18] which is similar to the results in this study. However, the efficiency drops significantly when AuNPs were applied to cell conditioned media (Figure 5). AuNPs can bind to cell membrane and internalized by the cells to the endocytic compartments,[9,11,19,39] thus being cleared away to some extend from the fluid. It is also likely that in multi-protein systems, such as cell culture supernatant, serum, or *in vivo* environment, nanoparticles are surrounded by a protein corona,[40] with which VEGF165 may compete to bind to AuNPs. The protein corona is a dynamic composition and structure determined by the orchestra of (1) the physicochemical properties of the particles (material, shape, surface area, charge, size, concentration), (2) the characteristics of the bio-fluid (protein constituents, abundancy, affinity to particles) and (3) the exposure (time, temperature, mechanics).[18,40–42] In binding to AuNPs, VEGF165 may occupy the position of lower abundant and/or affinitive proteins, but may give way to higher abundant and/or affinitive proteins. To improve the binding efficiency of nanoparticles to VEGF165 or other particular targets *in vivo*, it may be useful to optimize the physicochemical properties, dosage, or exposure timing of the particles, as our previous

work,[18] the results here, and some strategies to control the composition of protein corona[40] suggested.

AuNPs have been tested in a variety of *in vivo* models, among which are mice, rats, guinea pigs, rabbits, beagles and zebrafish, and are observed to be biocompatible in most cases.[43] In other words, the effects of the nanoparticles on normal cells and tissues can be limited and in favor of their using with proper indication, dosing and administration route. Indeed, while showing inhibition to the proliferation of ovarian and pancreatic cancer cells, AuNPs did not significantly affect the proliferation of normal epithelial cells, nor did they lead to systemic toxicity in the experimental animals.[11,19] Multiple observations have suggested that AuNPs inhibit pathological angiogenesis; however, evidence about what effects the nanoparticles on the process of normal angiogenesis is still lacking.

In conclusion, results presented here demonstrated that AuNPs possess the ability to disrupt multicellular crosstalk in the tumor microenvironment, which may be utilized to improve therapeutic outcome. Future investigation will focus on translating the *in vitro* finding to *in vivo* settings and the effects of gold nanoparticles on other TME cell phenotypes such as fibroblast activation.

Experimental Procedures

Isolation and Characterization of Primary Ovarian Cancer Associated Fibroblasts (CAFs).—Primary ovarian CAFs were isolated by the outgrowth method[44,45] from 26 freshly resected ovarian cancer tissues from patients undergoing surgery at the University of Oklahoma Health Sciences Center with approved Institutional Review Board protocol. Briefly, 0.5–1.5 mm^3 tissue blocks were cut with scissors after 4 washes of the tissues with sterile phosphate-buffered saline (PBS, 02-0119-0500, VWR, Radnor, PA), and were placed 7–8 pieces/well to 6-well plates (T1006, Thomas Scientific, Swedesboro, NJ) in the presence of DMEM/F12 (10–090, Corning, NY) supplemented with 15% Fetal Bovine Serum (FBS, 16000–044, Life technologies Carlsbad, CA) and 1% Penn-Strep (15140–122, Life technologies). Tissue blocks were maintained at 37 °C in a humidified 95% air and 5% CO_2 atmosphere and examined daily for the emergence of fibroblasts. Medium was changed every 24–48 h. CAFs grew out from the tissue blocks 2–3 days later and reached confluence in 2–3 weeks. The CAFs were named TAF1–26 according to tissue serial number. Cells were expanded to passage 4, verified by expression of α-SMA, fibronectin and E-cadherin by western botting and immunofluorescence staining, and stored in liquid nitrogen. TAF18 and TAF19 cells were used up to passage 6 in this study.

Cell Culture.—Human epithelial ovarian cancer cell lines (CCs) A2780-CP20 (CP20) was a kind gift from Dr. Anil K. Sood (MD Anderson Cancer Center, Houston, TX); OV90 was purchased from American Type Culture Collection (Manassas, VA); OVCAR4 was purchased from National Cancer Institute (Bethesda, MD). All the cells were grown in RPMI 1640 (10–040-CV, Corning) supplemented with 10% FBS and 1% Penn-Strep. Ovarian CAFs were grown in DMEM:F12 with 15% FBS and 1% Penn-Strep. Human umbilical vein endothelial cell (HUVEC, Lonza, Walkersville, MD) and human microvascular endothelial cells (HMEC, a kind gift from Professor Xin Zhang, OUHSC

Stephenson Cancer Center, OKC, OK)[46] were grown in Endothelial Cell Growth Medium-2 BulletKit (EGM, CC-3162), and used up to passage 6. All the cells were maintained at 37 °C in a humidified 95% air and 5% CO_2 atmosphere.

Preparation and Characterization of 20 nm AuNPs.—AuNPs (20 nm in diameter) were prepared as described previously.[11] Briefly, 5 ml 10 mM tetrachloroauric acid trihydrate ($HAuCl_4 \cdot 3H_2O$, 520918, Sigma-Aldrich, St. Louis, MO) in 185 ml endotoxin-free water (786671, G Biosciences, St. Louis, MO) was heated to boil with gently stirring in a 500 ml flask. 15 ml of 1% sodium citrate (1613859, Sigma-Aldrich) preheated to 70 °C was added rapidly to the flask 3–4 min later. The solution was allowed to boil for 12–15 minutes with vigorous stirring until the color becomes dark purple. The solution was then moved to room temperature and stirred overnight. The AuNPs were characterized using dynamic light scattering (DLS, Zetasizer Nano ZS, Malvern Panalytical, Malvern, UK), UV-Visible spectroscopy (Spectrostar Nano, BMG Labtech, Cary, NC), zeta potential measurements (Malvern Zetasizer Nano ZS), and transmission electron microscope (TEM, Hitachi H-7600, Chiyoda, Tokyo, Japan). The nanoparticles were concentrated by centrifugation at 10000 rpm at 10 °C for 20 min before using. To determine the concentration of nanoparticles prepared, the original solution was concentrated 16 times, and OD522 and OD800 were measured for both original and concentrated solutions. Concentration of the original preparation was calculated as: 30.018 × Total Initial Volume × (OD520-OD800) of As Concentrated / [As Synthesized Volume × (OD520-OD800) of As Synthesized].

Preparation of Conditioned Media (CM).—CM from untreated or AuNP-treated CCs, CAFs or ECs was prepared as described previously (Figure 2A).[19,47] Briefly, cells were seeded to 10 cm culture dishes (T1110, Thomas Scientific) so as to reach 60–70% confluent the next day when the media were replaced with serum-free RPMI 1640 for CCs, DMEM:F12 for CAFs, or Endothelial Cell Growth Basal Medium-2 (EBM, CC-3156, Lonza) for ECs. 24 h later, the media were replaced again with fresh serum-free media (SFM) and treated with 0, 20, or 40 μg/ml freshly prepared 20 nm AuNPs for 48 h. The media were collected, centrifuged at 1500 rpm for 5 min to remove cell debris, then centrifuged at 10000 rpm at 10 °C for 20 min to remove the remaining AuNPs, and stored at −80 C° or used freshly. The resulted CM were diluted with equal volume of fresh SFM before subsequent functional experiments, or not diluted for VEGF level determination and mechanism study.

***In vitro* Tube Formation Assay.—**HUVECs or HMECs were starved in EBM for 16 h before trypsinization with Trypsin-EDTA (0.25%, 25200072, ThermoFisher Scientific, Waltham, MA) and incubated for 30 min with CM. ECs were then seeded 20,000 cells/100μl/well (HUVEC) or 30,000 cells/100μl/well (HMEC) to 96-well plate (T1096, Thomas Scientific) coated with 50 μl Matrigel (1:1 diluted with EBM) (354234, Corning). Images of tubular network were taken 4 h later. Tube formation was evaluated by counting the branching points of the tubular network with ImageJ software (National Institutes of Health, Rockville, MD)[48]. EGM or PBS diluted with equal volume of EBM was used as positive or non-treatment control. Tube formation fold increase was calculated as: (CM treatment -

PBS)/PBS; decrease percentage: (CM Con - CM AuNPs)/CM Con × 100. Experiments were performed in triplicate and repeated 3 times.

Migration Assay.—HMECs or HUVECs were starved in EBM for 16 h, trypsinized and seeded to transwell (3422, Corning) at 100,000 cells/100μl/insert. ECs migration was induced by CM added to the outwells (3422, Corning) 700μl/well for 16 h. In co-culture system (Figure 2B), CCs, CAFs or ECs were seeded to outwells. The cells (70–80% confluent) were starved in SFM for 24 h and then treated with/without 40 μg/ml AuNPs in 700 μl fresh SFM for 36 h. Half volume of the media were replaced by fresh SFM immediately before placing the transwell inserts with starved ECs to the plates for migration for 16 h. Cells were then fixed and stained with 0.1% crystal violet (C0775, Sigma-Aldrich) and those inside the inserts were removed using a cotton swab. Cells migrated through the membrane were photographed and counted with ImageJ. 10% EGM or PBS diluted with equal volume of EBM was used as positive or non-treatment control. For quantification, migration by 10% EGM was set as 100%. Migration fold increase was calculated as: (CM treatment or co-culture - PBS)/PBS; decrease percentage: (Con - AuNPs)/Con × 100. Experiments were performed in duplicate and repeated 3 times.

Enzyme-linked Immunosorbent Assay (ELISA).—The clearance of extrogenous recombinant VEGF165 from its single-protein solution by AuNPs, and VEGF165 levels in cell CM were determined by Human VEGF Mini ABTS ELISA Development Kit (#900-M10, PeproTech, Rocky Hill, NJ). VEGF single-protein solutions were made by adding 1000 pg/ml recombinant VEGF165 (from the Kit) to 500ul RPMI 1640 SFM. AuNPs (0, 20, or 40 μg/ml) were then incubated in the solutions for 16 h with agitation. The samples were centrifuged at 10,000 rpm for 20 min at 10 °C, and the supernatants were collected. Cell CM were prepared as above. VEGF165 level in the supernatants and CM were measured following the manufacturer's protocol. Briefly, 0.5 μg/ml VEGF165 capture antibodies were coated to ELISA plate overnight. After blocking, samples, standard (recombinant VEGF165, diluted to 1000, 500, 250, 125, 62.5, 31.25, 15.625 pg/ml) and PBS were added, followed by incubation with 0.25 μg/ml VEGF165 detection antibodies, Avidin-HRP conjugates and ABTS substrate. Color development was monitored with plate reader (Spectrostar Nano, BMG Labtech) at 405 nm with wavelength correction at 650 nm. Experiments were performed in triplicate and repeated 3 times.

Immunofluorescence.—Cells were grown on coverslips (1217N78, Thomas Scientific), washed with PBS, fixed in 4% paraformaldehyde (AAJ19943K2, ThermoFisher) for 10 min at room temperature, washed, permeabilized with 0.2% Triton X-100 (X100, Sigma-Aldrich) for 10 min, and blocked with 2% bovine serum albumin (BSA, A2153, Sigma-Aldrich) in PBS for 30 min. The coverslips were incubated with primary antibodies overnight at 4°C, washed, and then incubated with secondary antibodies for 1 h at room temperature, followed by mounting with Vectashield with DAPI (H-1200, Vector Laboratories, Burlingame, CA). Fluorescence was observed using a Zeiss Axiovert 200m Inverted Fluorescent Microscope. Primary antibodies used in this study were: mouse-anti-Fibronectin (1:200, #610077, BD Biosciences, San Jose, CA), and rabbit-anti-α-SMA (1:200, ab5694, Abcam, Cambridge, MA). Secondary antibodies were: Alexa Fluor 568

conjugated goat anti-Mouse IgG (1:500, #A-21124, ThermoFisher), and Alexa Fluor 568 conjugated goat anti-Rabbit IgG (1:500, # A-11036, ThermoFisher).

Western Blotting.—For CAF and epithelial cell marker expression, TAFs cells at passage 3 were used. For detection of VEGF phosphorylation, HUVECs or HMECs were starved in EBM for 16 h, and then incubated for 5 min with CM from CCs, CAFs or ECs as detailed above. Recombinant human VEGF165 (#100–20, PeproTech) or PBS was used as positive or negative control. Media were removed, and cells were placed on ice, washed 3 times with cold PBS and lysed with RIPA buffer (BP-115, Boston BioProducts, Ashland, MA) containing Protease and Phosphatase Inhibitor Cocktail (78440, ThermoFisher). Lysate protein concentration was determined using BCA Protein Assay Kit (23227, ThermoFisher). Lysates (10–50 μg proteins/lane) were loaded to and separated on 6%–10% SDS-PAGE gel and electrophoretically transferred to PVDF membrane (1620177, Bio-Rad, Hercules, CA). The membranes were blocked in 4% BSA/PBST (0.1% Tween-20, P1379, Sigma-Aldrich, in PBS) at ambient temperature for 1 h, incubated with primary antibodies at 4°C for 16 h, followed by washing and incubation with HRP-coupled secondary antibodies for 1 h at room temperature. Signals were visualized with Clarity Western ECL Substrates (1705061, Bio-Rad) or SuperSignal West Femto (TI271896A, ThermoFisher). Blots were imaged with Color LaserJet Pro MFO M477fdn (HP, Palo Alto, CA). Primary antibodies used in this study were: mouse-anti-Fibronectin (1:1000, #610077, BD Biosciences), rabbit-anti-α-SMA (1:1000, ab5694, Abcam), mouse-anti-E-cadherin (1:1000, #610182, BD Biosciences), rabbit anti-GAPDH (1:10000, G9545, Sigma), rabbit anti-Phospho-VEGFR2 (Tyr1175) (1:200, #2478, Cell Signaling), rabbit anti-VEGFR2 (1:1000, #2479, Cell Signaling), and mouse-anti-HSP90 (1:10000, ab13492, Abcam). Secondary antibodies were: goat-anti-Rabbit-IgG (1:10000, A6154, Sigma) and goat-anti-Mouse-IgG (1:10000, A4416, Sigma).

Statistics.—Data are expressed as mean ± SEM. Statistics was performed using One-way ANOVA with Tukey's post-test. P value ≤0.05 was considered statistically significant.

Supplementary Material

Refer to Web version on PubMed Central for supplementary material.

ACKNOWLEDGMENT

This work was supported by National Institutes of Health Grant 1R01 CA220237-01A1, 2CA136494, CA213278 (to P.M.) and CA157481 (to R.B.) and 1R01HL120585 (to both PM and RB). We also thank the Peggy and Charles Stephenson Cancer Center at the University of Oklahoma Health Sciences Center for a seed grant and an Institutional Development Award (IDeA) from the National Institute of General Medical Sciences of the National Institutes of Health under grant number P20 GM103639 for the use of Histology and Immunohistochemistry Core, which provided immunohistochemistry and image analysis service.

Abbreviations

AuNP	gold nanoparticle
CAF	cancer associated fibroblast
CC	cancer cell

EBM	endothelial cell growth basal medium
EC	endothelial cell
EGM	endothelial cell growth medium
ELISA	enzyme linked immunosorbent assay
EOC	Epithelial ovarian cancer
HMEC	human microvascular endothelial cells
HUVEC	human umbilical vein endothelial cell
SFM	serum-free medium
TME	tumor microenvironment
VEGF	vascular endothelial growth factor

REFERENCES

(1). Siegel RL, Miller KD, and Jemal A (2019) Cancer statistics, 2019. Ca-Cancer J Clin 69, 7–34. [PubMed: 30620402]

(2). Kim J, Park EY, Kim O, Schilder JM, Coffey DM, Cho CH, and Bast RC Jr. (2018) Cell Origins of High-Grade Serous Ovarian Cancer. Cancers (Basel) 10(11).

(3). Thibault B, Castells M, Delord JP, and Couderc B (2014) Ovarian cancer microenvironment: implications for cancer dissemination and chemoresistance acquisition. Cancer Metastasis Rev 33, 17–39. [PubMed: 24357056]

(4). Bertero T, Oldham WM, Grasset EM, Bourget I, Boulter E, Pisano S, Hofman P, Bellvert F, Meneguzzi G, Bulavin DV, et al. (2019) Tumor-Stroma Mechanics Coordinate Amino Acid Availability to Sustain Tumor Growth and Malignancy. Cell Metab 29, 124–140 e10. [PubMed: 30293773]

(5). Lhomond S, Avril T, Dejeans N, Voutetakis K, Doultsinos D, McMahon M, Pineau R, Obacz J, Papadodima O, Jouan F, et al. (2018) Dual IRE1 RNase functions dictate glioblastoma development. EMBO Mol Med 10(3).

(6). Valkenburg KC, de Groot AE, and Pienta KJ (2018) Targeting the tumour stroma to improve cancer therapy. Nat Rev Clin Oncol 15, 366–381. [PubMed: 29651130]

(7). Balkwill FR, Capasso M, and Hagemann T (2012) The tumor microenvironment at a glance. J Cell Sci 125, 5591–6. [PubMed: 23420197]

(8). Bhattacharya R, P. C., Verma R, Kumar S, Greipp PR, Mukherjee P. . (2007) Gold Nanoparticles Inhibit the Proliferation of Multiple Myeloma Cells. Advanced Materials 19, 711–716.

(9). Tan G, and Onur MA (2018) Cellular localization and biological effects of 20nm-gold nanoparticles. J Biomed Mater Res A 106, 1708–1721. [PubMed: 29468810]

(10). Li W, Li X, Liu S, Yang W, Pan F, Yang XY, Du B, Qin L, and Pan Y (2017) Gold nanoparticles attenuate metastasis by tumor vasculature normalization and epithelial-mesenchymal transition inhibition. Int J Nanomedicine 12, 3509–3520. [PubMed: 28496326]

(11). Arvizo RR, Saha S, Wang EF, Robertson JD, Bhattacharya R, and Mukherjee P (2013) Inhibition of tumor growth and metastasis by a self-therapeutic nanoparticle. P Natl Acad Sci USA 110, 6700–6705.

(12). Lo HM, Ma MC, Shieh JM, Chen HL, and Wu WB (2018) Naked physically synthesized gold nanoparticles affect migration, mitochondrial activity, and proliferation of vascular smooth muscle cells. Int J Nanomed 13, 3163–3176.

(13). Shen N, Zhang R, Zhang HR, Luo HY, Shen W, Gao X, Guo DZ, and Shen J (2018) Inhibition of retinal angiogenesis by gold nanoparticles via inducing autophagy. Int J Ophthalmol-Chi 11, 1269–1276.

(14). Kim JH, Kim MH, Jo DH, Yu YS, Lee TG, and Kim JH (2011) The inhibition of retinal neovascularization by gold nanoparticles via suppression of VEGFR-2 activation. Biomaterials 32, 1865–1871. [PubMed: 21145587]

(15). Roh YJ, Rho CR, Cho WK, and Kang S (2016) The Antiangiogenic Effects of Gold Nanoparticles on Experimental Choroidal Neovascularization in Mice. Invest Ophth Vis Sci 57, 6561–6567.

(16). Mukherjee P, Bhattacharya R, Wang P, Wang L, Basu S, Nagy JA, Atala A, Mukhopadhyay D, and Soker S (2005) Antiangiogenic properties of gold nanoparticles. Clin Cancer Res 11, 3530–4. [PubMed: 15867256]

(17). Bhattacharya R, and Mukherjee P (2008) Biological properties of “naked” metal nanoparticles. Adv Drug Deliv Rev 60, 1289–306. [PubMed: 18501989]

(18). Arvizo RR, Rana S, Miranda OR, Bhattacharya R, Rotello VM, and Mukherjee P (2011) Mechanism of anti-angiogenic property of gold nanoparticles: role of nanoparticle size and surface charge. Nanomed-Nanotechnol 7, 580–587.

(19). Saha S, Xiong X, Chakraborty PK, Shameer K, Arvizo RR, Kudgus RA, Dwivedi SK, Hossen MN, Gillies EM, Robertson JD, et al. (2016) Gold Nanoparticle Reprograms Pancreatic Tumor Microenvironment and Inhibits Tumor Growth. Acs Nano 10, 10636–10651. [PubMed: 27758098]

(20). Patra CR, Bhattacharya R, Wang E, Katarya A, Lau JS, Dutta S, Muders M, Wang S, Buhrow SA, Safgren SL, et al. (2008) Targeted delivery of gemcitabine to pancreatic adenocarcinoma using cetuximab as a targeting agent. Cancer Res 68, 1970–8. [PubMed: 18339879]

(21). De Palma M, Biziato D, and Petrova TV (2017) Microenvironmental regulation of tumour angiogenesis. Nat Rev Cancer 17, 457–474. [PubMed: 28706266]

(22). Ronca R, Van Ginderachter JA, and Turtoi A (2018) Paracrine interactions of cancer-associated fibroblasts, macrophages and endothelial cells: tumor allies and foes. Curr Opin Oncol 30, 45–53. [PubMed: 29084000]

(23). Choi H, and Moon A (2018) Crosstalk between cancer cells and endothelial cells: implications for tumor progression and intervention. Arch Pharm Res 41, 711–724. [PubMed: 29961196]

(24). Xiong X, Arvizo RR, Saha S, Robertson DJ, McMeekin S, Bhattacharya R, and Mukherjee P (2014) Sensitization of ovarian cancer cells to cisplatin by gold nanoparticles. Oncotarget 5, 6453–65. [PubMed: 25071019]

(25). Kalluri R (2016) The biology and function of fibroblasts in cancer. Nat Rev Cancer 16, 582–98. [PubMed: 27550820]

(26). Kalluri R, and Weinberg RA (2009) The basics of epithelial-mesenchymal transition. J Clin Invest 119, 1420–8. [PubMed: 19487818]

(27). Nurmik M, Ullmann P, Rodriguez F, Haan S, and Letellier E (2019) In search of definitions: Cancer-associated fibroblasts and their markers. Int J Cancer

(28). Gong YX, Scott E, Lu R, Xu Y, Oh WK, and Yu Q (2013) TIMP-1 Promotes Accumulation of Cancer Associated Fibroblasts and Cancer Progression. Plos One 8(10).

(29). Zeisberg M, and Neilson EG (2009) Biomarkers for epithelial-mesenchymal transitions. Journal of Clinical Investigation 119, 1429–1437. [PubMed: 19487819]

(30). van Roy F, and Berx G (2008) The cell-cell adhesion molecule E-cadherin. Cell Mol Life Sci 65, 3756–3788. [PubMed: 18726070]

(31). Ferrara N, Gerber HP, and LeCouter J (2003) The biology of VEGF and its receptors. Nat Med 9, 669–76. [PubMed: 12778165]

(32). Simons M, Gordon E, and Claesson-Welsh L (2016) Mechanisms and regulation of endothelial VEGF receptor signalling. Nat Rev Mol Cell Biol 17, 611–25. [PubMed: 27461391]

(33). Carmeliet P (2005) Angiogenesis in life, disease and medicine. Nature 438, 932–6. [PubMed: 16355210]

(34). Albini A, Bruno A, Noonan DM, and Mortara L (2018) Contribution to Tumor Angiogenesis From Innate Immune Cells Within the Tumor Microenvironment: Implications for Immunotherapy. Front Immunol 9, 527. [PubMed: 29675018]

(35). Liu Y, Cox SR, Morita T, and Kourembanas S (1995) Hypoxia regulates vascular endothelial growth factor gene expression in endothelial cells. Identification of a 5' enhancer. Circ Res 77, 638–43. [PubMed: 7641334]

(36). Namiki A, Brogi E, Kearney M, Kim EA, Wu T, Couffinhal T, Varticovski L, and Isner JM (1995) Hypoxia induces vascular endothelial growth factor in cultured human endothelial cells. J Biol Chem 270, 31189–95. [PubMed: 8537383]

(37). Marti HH, and Risau W (1998) Systemic hypoxia changes the organ-specific distribution of vascular endothelial growth factor and its receptors. Proc Natl Acad Sci U S A 95, 15809–14. [PubMed: 9861052]

(38). Cannizzo CM, Adonopulos AA, Solly EL, Ridiandries A, Vanags LZ, Mulangala J, Yuen SCG, Tsatralis T, Henriquez R, Robertson S, et al. (2018) VEGFR2 is activated by high-density lipoproteins and plays a key role in the proangiogenic action of HDL in ischemia. FASEB J 32, 2911–2922. [PubMed: 29401597]

(39). Jiang Y, Huo S, Mizuhara T, Das R, Lee YW, Hou S, Moyano DF, Duncan B, Liang XJ, and Rotello VM (2015) The Interplay of Size and Surface Functionality on the Cellular Uptake of Sub-10 nm Gold Nanoparticles. ACS Nano 9, 9986–93. [PubMed: 26435075]

(40). Mahmoudi M, Bertrand N, Zope H, and Farokhzad OC (2016) Emerging understanding of the protein corona at the nano-bio interfaces. Nano Today 11, 817–832.

(41). Rezaei G, Daghighi SM, Haririan I, Yousefi I, Raoufi M, Rezaee F, and Dinarvand R (2019) Protein corona variation in nanoparticles revisited: A dynamic grouping strategy. Colloids Surf B Biointerfaces 179, 505–516. [PubMed: 31009853]

(42). Pozzi D, Caracciolo G, Digiacomo L, Colapicchioni V, Palchetti S, Capriotti AL, Cavaliere C, Zenezini Chiozzi R, Puglisi A, and Lagana A (2015) The biomolecular corona of nanoparticles in circulating biological media. Nanoscale 7, 13958–66. [PubMed: 26222625]

(43). Masse F, Ouellette M, Lamoureux G, and Boisselier E (2019) Gold nanoparticles in ophthalmology. Med Res Rev 39, 302–327. [PubMed: 29766541]

(44). Bachem MG, Schneider E, Gross H, Weidenbach H, Schmid RM, Menke A, Siech M, Beger H, Grunert A, and Adler G (1998) Identification, culture, and characterization of pancreatic stellate cells in rats and humans. Gastroenterology 115, 421–432. [PubMed: 9679048]

(45). Zhang Y, Tang H, Cai J, Zhang T, Guo J, Feng D, and Wang Z (2011) Ovarian cancer-associated fibroblasts contribute to epithelial ovarian carcinoma metastasis by promoting angiogenesis, lymphangiogenesis and tumor cell invasion. Cancer Lett 303, 47–55. [PubMed: 21310528]

(46). Huang C, Fu C, Wren JD, Wang X, Zhang F, Zhang YH, Connel SA, Chen T, and Zhang XA (2018) Tetraspanin-enriched microdomains regulate digitation junctions. Cell Mol Life Sci 75, 3423–3439. [PubMed: 29589089]

(47). Straussman R, Morikawa T, Shee K, Barzily-Rokni M, Qian ZR, Du JY, Davis A, Mongare MM, Gould J, Frederick DT, et al. (2012) Tumour micro-environment elicits innate resistance to RAF inhibitors through HGF secretion. Nature 487, 500–4. [PubMed: 22763439]

(48). Zhang YS, and Daaka Y (2011) PGE2 promotes angiogenesis through EP4 and PKAC gamma pathway. Blood 118, 5355–5364. [PubMed: 21926356]

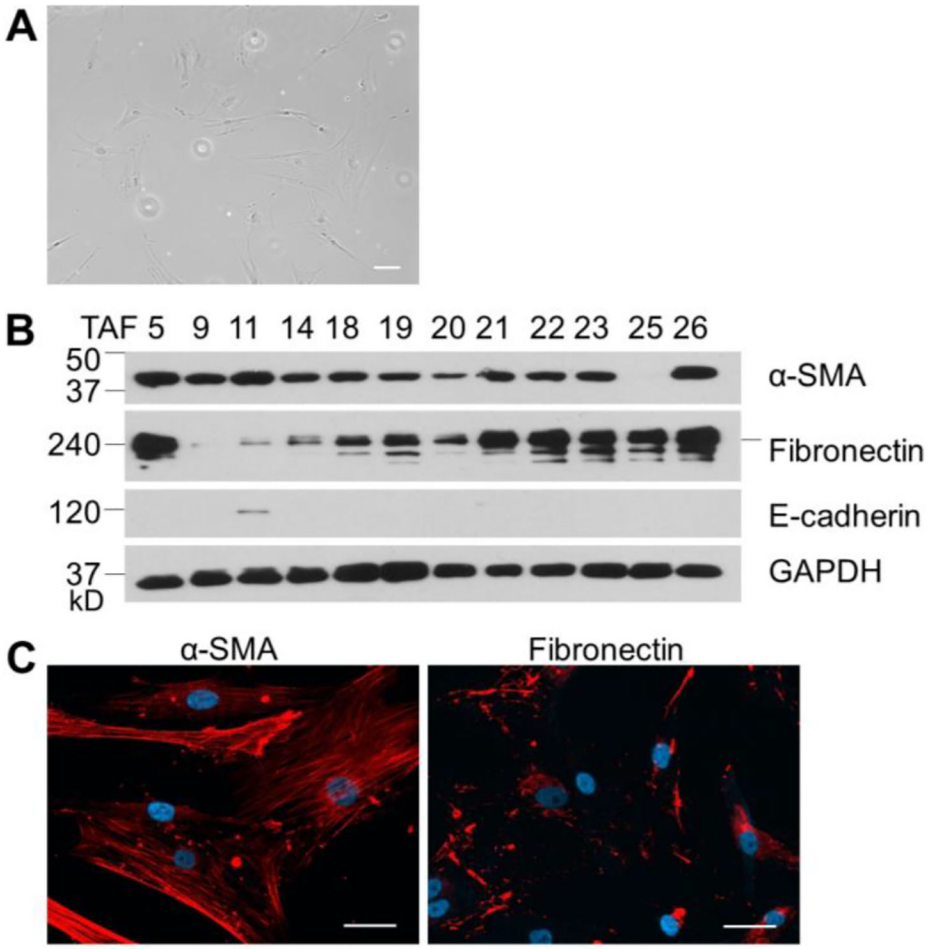

Figure 1.

Isolation and characterization of ovarian CAFs. (A) Ovarian CAFs were isolated by out-growth method from 26 freshly resected ovarian tumors. Some large, flat, spindle-shaped cells grew out of 15 tissue blocks 2–3 days after the placing of tissue to culture plates. Scale bar: 10 μm. (B) Cells were expanded to passage 4 and subjected to western botting for expression of α-SMA, Fibronectin and E-cadherin. GAPDH was used as loading control. (C) Cells were subjected to immunofluorescence staining for α-SMA and Fibronectin. Shown are TAF18. Scale bar: 10 μm.

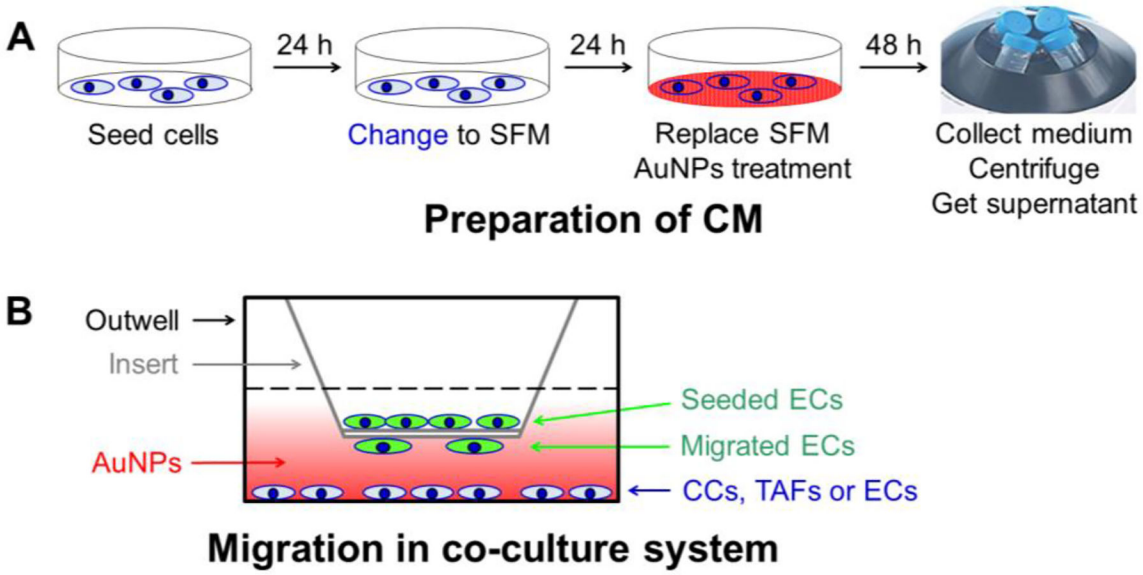

Figure 2.

Schematic view of (A) preparation of conditioned media and (B) Migration assay in co-culture system. (A) Cells were seeded at day 1, and the media were replaced with SFM at day 2. The media were replaced again with SFM at day 3 and treated with or without AuNPs for another 2 days. The media were collected, centrifuged to remove cell debris and AuNPs, and stored at −80C° or used freshly. (B) The migration-inducing cells were seeded on outwell, treated with or without AuNPs in SFM for 36h, and then co-cultured with ECs seeded to the inserts for 16 h. ECs migrated to the outside of the insert were then evaluated.

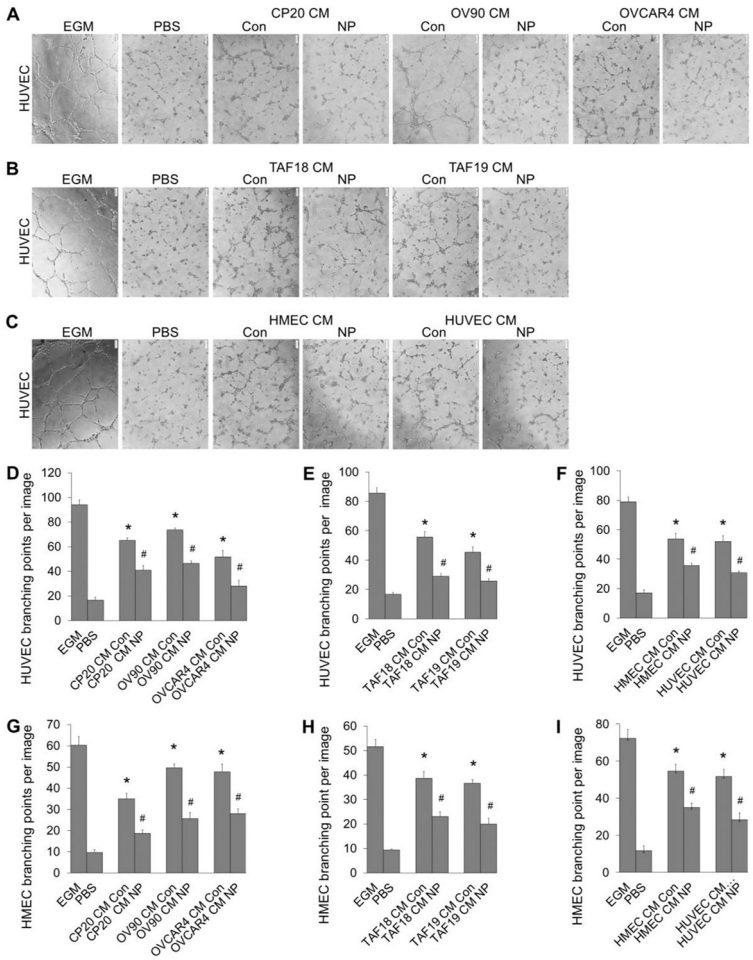

Figure 3.

Tube formation of EC treated with CM from CCs, CAFs or ECs. CM were diluted with equal volume of fresh EBM before use. HUVECs or HMECs were starved in EBM for 16 h before trypsinized and incubated for 30 min with the CM. ECs were then seeded 20,000 cells/well (HUVEC) or 30,000 cells/well (HMEC) to 96-well plate coated with 50 μl Matrigel (1:1 diluted with EBM). Images of tubular network were taken 4 h later. Tube formation was evaluated by counting the branching points of the tubular network with ImageJ. EGM or PBS diluted with equal volume of EBM was used as positive or non-treatment control. (A-C) Typical images of tube formation of HUVECs treated with CM of CCs, CAFs or ECs. (D-F) Quantification of HUVEC tube formation. (G-l) Quantification of HMEC tube formation. Experiments were performed in triplicate and repeated 3 times with similar results. Con: control, NP: AuNPs. Scale bar: 100 μm. *, $p<0.05$, compare to PBS: #, $p<0.05$, compare to corresponding Con.

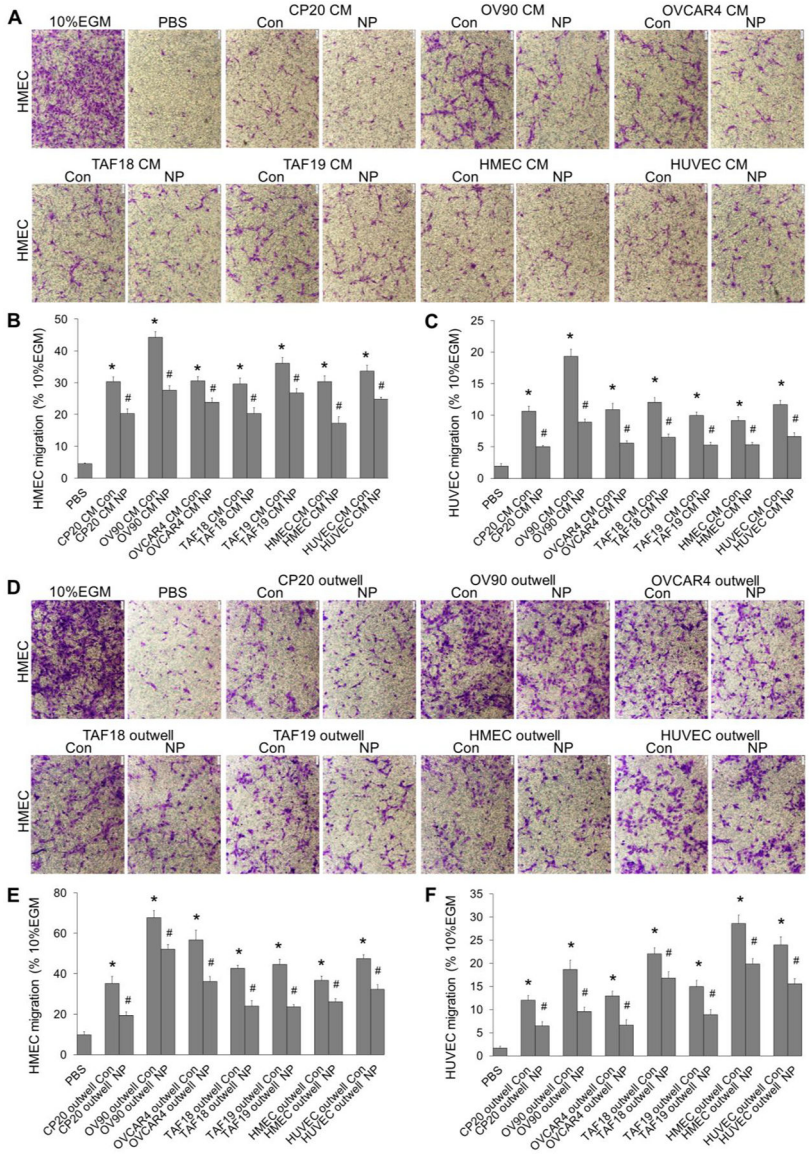

Figure 4.

Migration of ECs treated with cell CM, or co-cultured with cells treated with AuNPs. (A-C) HMECs or HUVECs were starved in EBM for 16 h before trypsinized and seeded 100,000 cells/insert in Boyden chamber system. ECs migration was induced by CM for 16 h. Cells migrated through the membrane were photographed (A, HMEC) and counted (B, HMEC; C, HUVEC). (D-F) CP20, OV90, OVCAR4, TAF18, TAF19, HMEC or HUVEC cells were seeded to 24-well plates. Cells (70–80% confluent) were starved in SFM for 24 h and then treated with or without 40 μg/ml AuNPs in for 36 h. Half volume of the media were replaced by fresh SFM immediately before assay. Starved HMECs or HUVECs were trypsinized and seeded 100,000 cells to each transwell insert. The inserts were then placed to 24-well plates where the outwell cells were being treated with or without AuNPs. HMEC (D, E) or HUVEC (F) cell migration was induced for 16 h and evaluated. 10% EGM or PBS diluted with equal volume of EBM was used as positive or non-treatment control. Migration of 10%

EGM was set as 100%. Experiments were performed in duplicate and repeated 3 times. Con: control, NP: AuNPs. Scale bar: 100 μm. *, $p<0.05$, compare to PBS; #, $p<0.05$, compare to corresponding Con.

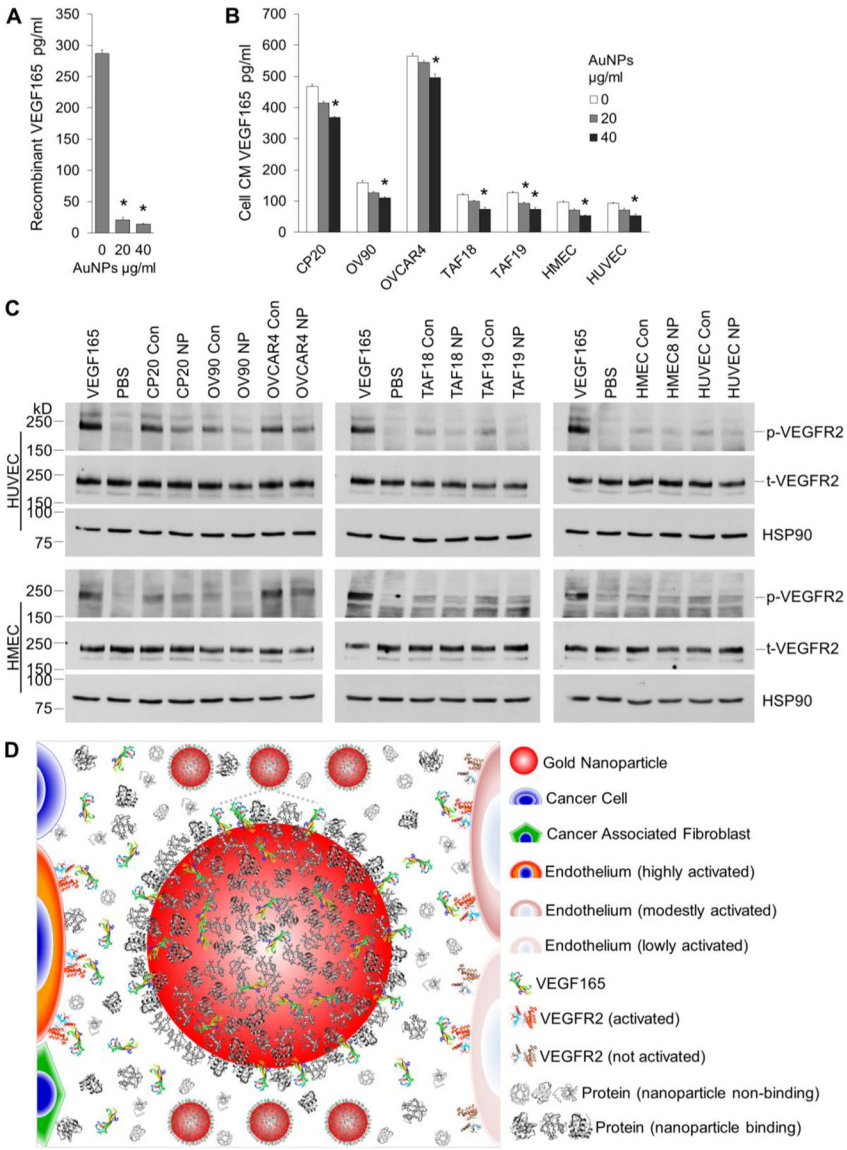

Figure 5.

VEGF quantification and signaling. (A) 1000pg/ml recombinant VEGF165 was incubated with 0, 20 or 40 μg/ml AuNPs for 16 h with agitation. VEGF165 levels in the supernatant were determined by ELISA. (B) Starved CC, CAF, or EC cells were incubated with 0, 20 or 40 μg/ml AuNP for 48 h. VEGF165 levels in CM were determined. (A, B) Experiments were performed in triplicate and repeated 3 times. *, $p<0.05$, compare to 0 μg/ml AuNPs. (C) Starved HUVECs or HMECs were treated with cell CM for 5 min before cell lysate preperation and protein concentration determination. Lysate with 20/40 μg HUVEC/HMEC proteins were loaded to each well in 6% SDS-PAGE gels. Equal amount of protein was loaded for phosphorylated VEGFR2 (p-VEGFR2) or total VEGFR2 (t-VEGFR2) in separate gels. HSP90 were used as loading control for phosphorylated VEGFR2. Recombinant human VEGF165 or PBS was used as positive or negative control. Experiments were repeated 3 times with similar results. Con: control CM, NP: AuNPs CM. (D) Schematic

representation of the role of AuNPs in signal transduction from TME cells to ECs. TME cells secret VEGF165 and other proteins. VEGF165 binds to VEGFR2 on EC surface, phosphorylates the receptors and induces EC migration and angiogenesis. In the presence of AuNPs, VEGF165 competes with protein corona to bind to AuNPs, and less amount is available to bind to and activate VEGFR2 on ECs, leading to decreased migration and angiogenesis. Drawing not to the scale.